JACS
JOURNAL OF THE AMERICAN CHEMICAL SOCIETY

Article

pubs.acs.org/JACS

# Ultrabright Luminescence from Gold Nanoclusters: Rigidifying the Au(I)−Thiolate Shell

Kyunglim Pyo,[†,§] Viraj Dhanushka Thanthirige,[‡,§] Kyuju Kwak,[†] Prabhu Pandurangan,[†] Guda Ramakrishna,*[,‡] and Dongil Lee*[,†]

[†]Department of Chemistry, Yonsei University, Seoul 120-749, Korea

[‡]Department of Chemistry, Western Michigan University, Kalamazoo Michigan 49008, United States

Supporting Information

**ABSTRACT:** Luminescent nanomaterials have captured the imagination of scientists for a long time and offer great promise for applications in organic/inorganic light-emitting displays, optoelectronics, optical sensors, biomedical imaging, and diagnostics. Atomically precise gold clusters with well-defined core−shell structures present bright prospects to achieve high photoluminescence efficiencies. In this study, gold clusters with a luminescence quantum yield greater than 60% were synthesized based on the $Au_{22}(SG)_{18}$ cluster, where SG is glutathione, by rigidifying its gold shell with tetraoctylammonium (TOA) cations. Time-resolved and temperature-dependent optical measurements on $Au_{22}(SG)_{18}$ have shown the presence of high quantum yield visible luminescence below freezing, indicating that shell rigidity enhances the luminescence quantum efficiency. To achieve high rigidity of the gold shell, $Au_{22}(SG)_{18}$ was bound to bulky TOA that resulted in greater than 60% quantum yield luminescence at room temperature. Optical measurements have confirmed that the rigidity of gold shell was responsible for the luminescence enhancement. This work presents an effective strategy to enhance the photoluminescence efficiencies of gold clusters by rigidifying the Au(I)−thiolate shell.

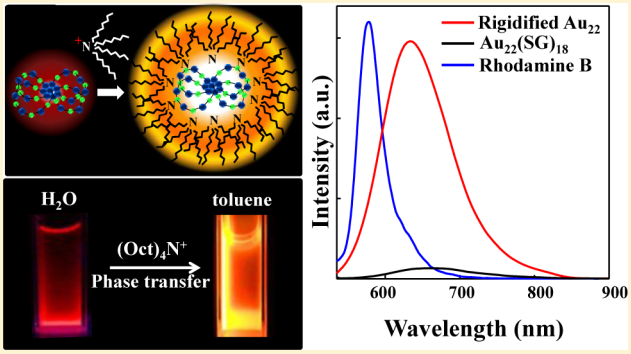


## INTRODUCTION

Ultrabright luminescent nanomaterials have received tremendous research attention for their applications in light-emitting diode displays, luminescent sensors, and biological imaging.[1−5] Greater photostability, low toxicity, and higher photoluminescence (PL) are quite essential for successful applications of such nanomaterials. Until recently, semiconductor quantum dots were at the focal point of research for these applications, and tremendous progress has been made with them.[1−5] However, the semiconductor quantum dots are relatively large and often toxic, limiting their applicability.[6−8] On the other hand, luminescent metal clusters have received much attention recently as alternatives to quantum dots and organic dye molecules for many technological applications due to the promises offered by their ultrafine size, excellent stability, and low toxicity.[9−17] However, the luminescence quantum yields (QY) from metal clusters are still not sufficiently high enough to offer practical applications.

High QY visible luminescence from gold clusters formed in dendrimers has been reported.[18,19] However, the origin of luminescence in them still remains unclear. The synthesis of atomically precise gold clusters, and consequent structural characterization, has ignited numerous research efforts[17−25] in order to achieve greater luminescence from gold clusters. However, the luminescence efficiencies reported for these clusters remain low with a significant amount of work focused on $Au_{25}$ clusters.[13,14] In a recent work, Xie and co-workers[26,27] have synthesized $Au_{22}(SG)_{18}$ clusters and shown emission around 665 nm with a QY of ∼8%. From the comparison of its luminescence properties with those of Au(I)−thiolate complexes that exhibit solvent-induced and cation-induced aggregation, the enhanced luminescence was ascribed to aggregation-induced emission (AIE).[26,27] However, the origin of emission in these clusters still remains unaddressed, posing a major hurdle for the development of highly luminescent clusters.

In this report, we present a novel strategy to dramatically enhance the luminescence efficiency of gold clusters based on the unique core−shell structure of $Au_{22}(SG)_{18}$. We have probed the origin of luminescence in $Au_{22}(SG)_{18}$ clusters with combined time-resolved and temperature-dependent luminescence techniques. Our investigations have shown that luminescence arises from the ligand-to-metal−metal charge transfer state of the gold shell and also unearthed an interestingly high QY triplet state in frozen media. As it was possible to observe ultrabright emission from these clusters in frozen media, $Au_{22}(SG)_{18}$ was bound to bulky TOA to rigidify

**Received:** April 23, 2015
**Published:** June 10, 2015




DOI: 10.1021/jacs.5b04210
J. Am. Chem. Soc. 2015, 137, 8244−8250

the Au(I)−thiolate shell. The luminescence efficiency of the rigidified $Au_{22}$ clusters is enhanced remarkably and exhibits high QY luminescence (>60%) at room temperature.

## RESULTS AND DISCUSSION

$Au_{22}(SG)_{18}$ clusters were synthesized following a literature procedure[25] with some modifications (see Experimental Section for experimental details). Briefly, instead of the carbon monoxide reduction method,[27] we synthesized $Au_{22}(SG)_{18}$ in ambient conditions using $NaBH_4$ as a reducing agent. The key to this synthesis was to slow the reduction reaction of the Au(I)−thiolate precursor. To moderate the reduction activity of $NaBH_4$, pH was initially adjusted to 12 to induce slow reduction of the Au(I)−thiolate precursor for 30 min before being changed to 2.5 to quench the $BH_4^-$ activity. We found that the pH control was critical for the high-yield preparation of $Au_{22}(SG)_{18}$. When the synthesis was run at pH 12 throughout the whole reaction, the yield of $Au_{22}(SG)_{18}$ clusters was greatly reduced and larger-sized gold nanoparticles were obtained. In addition, the yield of $Au_{22}(SG)_{18}$ was found to be the highest when the solution was stirred for 6 h. A polyacrylamide gel electrophoresis (PAGE) analysis of the reaction product shown in Supporting Information (SI) Figure S1 showed that there were three clusters, $Au_{15}(GS)_{13}$, $Au_{18}(GS)_{14}$, and $Au_{22}(GS)_{18}$, formed after being stirred for 2 h. During the additional stirring for 4 h, these clusters were focused to $Au_{15}(GS)_{13}$ and $Au_{22}(GS)_{18}$ clusters. The yield of $Au_{22}(SG)_{18}$ was found to decrease for a longer stirring time, and thus the reaction was run for 6 h. After solvent fractionation of the raw product using water/isopropyl alcohol (IPA) mixtures, highly pure red-emitting clusters were obtained with a typical yield of ∼10% on the basis of gold atoms. Transmission electron microscopy (TEM) image of the separated $Au_{22}(SG)_{18}$ in SI Figure S2 shows that the clusters are very monodispersed with an average core size of around 1.3 nm.

The negative-mode electrospray ionization (ESI) mass spectrum shown in Figure 1a firmly establishes that the isolated cluster is highly monodispersed and its chemical composition is consistent with $Au_{22}(SG)_{18}$. There are peaks observed at $m/z$ 1960−1990 that represent $Au_{22}(SG)_{18}$ ions containing a different number of $Na^+$ ions. The experimental isotope pattern for the most intense peak at $m/z$ ∼1968 Da was superimposed with the simulated one of $[Au_{22}(SG)_{18}\text{-}5H]^{5-}$, as compared in Figure 1a, inset. Shown in Figure 1b,c are the optical absorption and the emission and excitation spectra of $Au_{22}(SG)_{18}$ clusters in water. The emission maximum was found to be around 665 nm, and the excitation peaks at 470 and 520 nm match the most prominent maxima in the absorption spectra. The luminescence QY calibrated with Rhodamine B as the standard was found to be 7% for $Au_{22}(SG)_{18}$ in water.

To understand the excited state relaxation dynamics of $Au_{22}(SG)_{18}$ clusters, time-resolved photoluminescence measurements were carried out. In a previous study, we have shown that the luminescence from quantum-sized gold clusters consists of two components: a weak, low quantum yield visible luminescence followed by near-infrared luminescence.[28−30] The visible luminescence relaxes in ultrafast time scales and was assigned to gold core luminescence. To monitor the visible luminescence dynamics of $Au_{22}$ clusters, femtosecond measurements were carried out after excitation at 400 nm and monitoring at 520−550 nm (SI Figure S3). The luminescence decay traces were fit with 200 fs (>95%) and a picosecond relaxation time (<5%). The 200 fs decay component is assigned

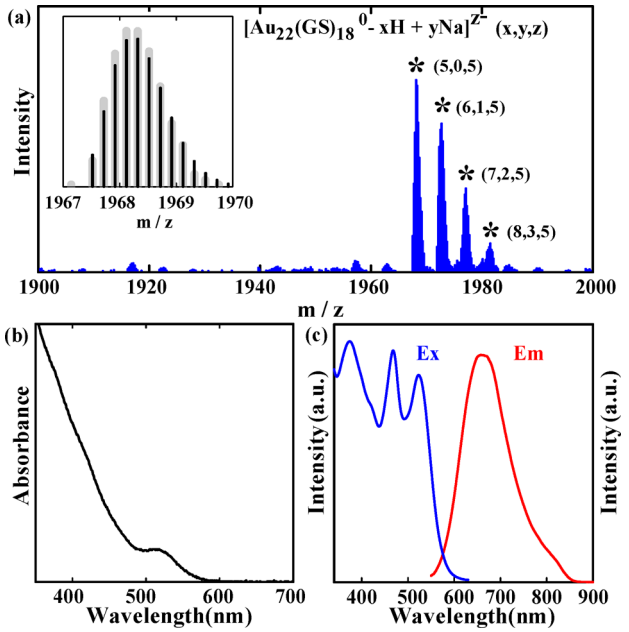


**Figure 1.** (a) ESI mass spectrum of $Au_{22}(SG)_{18}$ clusters obtained from the synthesis. The inset shows a comparison between the experimental data (gray line) and the calculated isotope pattern (black line) of $[Au_{22}(SG)_{18}\text{-}5H]^{5-}$. (b) Absorption spectrum and (c) excitation and emission spectra of $Au_{22}(SG)_{18}$ in water.

to the relaxation of gold core to gold shell or to the relaxation within gold core states, which then undergoes intersystem crossing to populate the triplet states of the gold shell. Other quantum-sized gold clusters have also shown similar ultrafast luminescence at this wavelength region, which was assigned to the relaxation of the gold core to the gold shell.[28−30] Femtosecond luminescence anisotropy measurements have shown zero anisotropy for the visible luminescence, indicating that the excitation and luminescence decay are dominantly localized on gold core states.

The most interesting aspect of luminescence from $Au_{22}(SG)_{18}$ clusters is the high quantum yield near-infrared luminescence with a maximum at 665 nm. Nanosecond time-resolved luminescence monitored at 670 nm for $Au_{22}(SG)_{18}$ in water has shown slow and multiexponential decay with lifetimes of 8 ns (49.2%), 130 ns (20.5%), 1.2 μs (28.5%), and >5 μs (1.9%). An average lifetime of 380 ns was determined for the luminescence decay at 670 nm (SI Figure S4). Similar longer lifetimes for luminescence at near-infrared were observed for $Au_{25}(SR)_{18}^-$ clusters and were attributed to the luminescence arising from gold shell states, where significant ligand contribution is present.[11−13] Also, long-lived luminescence was observed for Au(I)−thiolate complexes.[26]

To further investigate the origin of luminescence in $Au_{22}$ clusters, temperature-dependent luminescence measurements were carried out. Figure 2a shows the luminescence spectral change as temperature is decreased from 303 K to 77 K for $Au_{22}(SG)_{18}$ clusters in a 65:35 (v/v) glycerol−water mixture. This solvent mixture was chosen as it gave a decent glass at low temperatures. It is observed from Figure 2a that the luminescence intensity has increased with decreasing temperature along with a shift in the luminescence maximum from 670 to 580 nm. The inset of Figure 2a shows the change in luminescence maximum (black circles) as well as normalized luminescence intensity (red circles) as a function of temper-


DOI: 10.1021/jacs.5b04210
J. Am. Chem. Soc. 2015, 137, 8244−8250

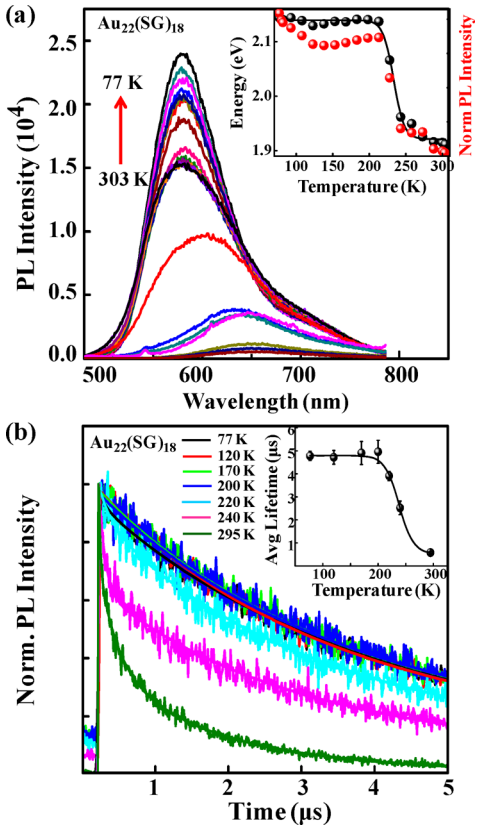


**Figure 2.** (a) Temperature-dependent photoluminescence spectra of $Au_{22}(SG)_{18}$ clusters at different temperatures. Inset shows the plot of PL maximum (black circles) and normalized PL intensity (red circles) as a function of temperature. (b) PL decay traces of $Au_{22}(SG)_{18}$ clusters as a function of temperature. Inset shows the average lifetime as a function of temperature.

ature. Interestingly, both show drastic increase around 233 K that corresponds to the freezing point of the solvent mixture.[31] Temperature-dependent luminescence decay traces and corresponding lifetimes of $Au_{22}(SG)_{18}$ clusters have also shown a sharp increase at a temperature of 233 K (Figure 2b and its inset). The luminescence decay at 77 K was fitted with a biexponential function, and an average lifetime determined from the analysis was increased by more than 12-fold from 380 ns at 295 K to 4.75 $\mu$s at 77 K. The observed microsecond-scale lifetime and large Stokes shift suggest that the emission from $Au_{22}(SG)_{18}$ clusters is mainly phosphorescence whose efficiency dramatically increases in the frozen media.

The long-lived luminescence observed for the $Au_{22}(SG)_{18}$ cluster was attributed to AIE by Xie and co-workers[27] as similar luminescence was observed for Au(I)−thiolate complexes in which the degree of aggregation was found to be affected by the solvent polarity or the presence of cations.[26,27] In the present work, however, it is unlikely that the degree of aggregation changes with lowering temperature for such a well-defined, isolated cluster as $Au_{22}(SG)_{18}$. A density functional theory (DFT) calculation predicts that the most stable isomer of the $Au_{22}(SG)_{18}$ cluster has a prolate $Au_8$ core protected by two trimer (GS-[Au-SG]$_3$) motifs and two tetramer (GS-[Au-SG]$_4$) motifs.[27] The trimer and tetramer form an interlocked gold shell structure. Based on this structural model, the long-lived, high quantum yield luminescence observed for $Au_{22}(SG)_{18}$ clusters can be better ascribed to ligand-to-metal−metal charge transfer (LMMCT) relaxation occurring at a triplet metal-centered state in the long, interlocked gold shell. The LMMCT-induced luminescence has been observed for a number of gold complexes and ascribed to aurophilic interactions that become important when the adjacent gold−gold distances are less than 3.6 Å.[32,33]

Temperature-dependent luminescence decay traces show an increase in LMMCT luminescence upon freezing, suggesting drastic reduction in the nonradiative relaxation offered by the gold shell. In addition to the enhanced luminescence below the freezing point, it is interesting to see that the luminescence maximum also shifted to a higher energy and the luminescence lifetime increased drastically. These observations unequivocally suggest that there is another triplet state which becomes prominent in frozen media. Taken together, the luminescence dynamics of the $Au_{22}(SG)_{18}$ cluster can be described as the following (Figure 3). Upon photoexcitation, the excited state of

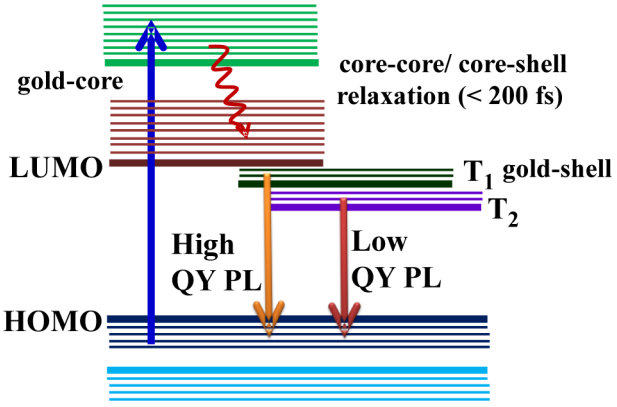


**Figure 3.** Schematic diagram showing the excited state relaxation dynamics in $Au_{22}(SG)_{18}$ clusters in water. $T_1$ and $T_2$ represent LMMCT states of the gold shell. $T_2$ states are destabilized by freezing or rigidifying the gold shell.

$Au_{22}(SG)_{18}$ relaxes very fast within gold core states or from the gold core to gold shell state. After fast intersystem crossing, the singlet state relaxes to a highly luminescent (LMMCT) triplet state ($T_1$), which then relaxes to a low energy and less luminescent triplet (LMMCT, $T_2$) state. The $T_2$ state possesses significant charge transfer (CT) characteristics that can be stabilized in polar media, and the interaction and fluctuation of the gold shell with the surrounding media leads to efficient nonradiative relaxation. As the gold shell becomes rigid in frozen media, the $T_2$ state is destabilized under reduced solvent interactions and the luminescence predominantly arises from the highly luminescent $T_1$ state. The $T_1$ state appears to be an intrinsic luminescent state of the gold shell and is not influenced by nonradiative relaxation channels of solvent or ligand fluctuations. These two LMMCT triplet states ($T_1$ and $T_2$) observed for $Au_{22}(SG)_{18}$ are analogous to the intramolecular charge transfer (ICT) states observed in organic luminophors. Organic molecules such as 7-amino coumarin derivatives[34] and branched donor-$\pi$-acceptor chromophores[35−37] possess both intrinsic ICT states and solvent-stabilized ICT states. Solvent-stabilized ICT states are stabilized in polar solvents and exhibit fluorescence quantum yields much lower than those of the intrinsic ICT states.[34−37]

Temperature-dependent luminescence evidently confirms that the rigidity of the gold shell is critical for the observation of ultrabright emission from the $Au_{22}$ clusters. Luminescence enhancement due to rigidity in organic molecules is very well


DOI: 10.1021/jacs.5b04210
J. Am. Chem. Soc. 2015, 137, 8244−8250

documented,[38,39] and it is intriguing to observe similar behavior for quantum-sized gold clusters. Then, a question arose, is it possible to rigidify the gold shell by other means and observe similarly bright luminescence from these clusters? To explore this possibility, $Au_{22}(SG)_{18}$ was ion paired with bulky TOA cations that bind with the carboxylate anions of glutathione.[40] Significant intramolecular interaction is expected between the alkyl chains of TOA cations, making the Au(I)−thiolate shell rigid, as depicted in Figure 4a. The electrostatic attraction

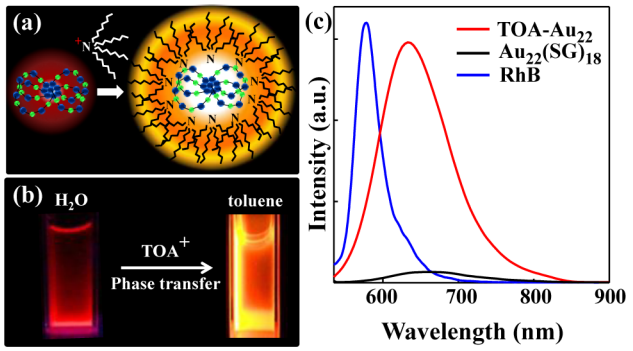


**Figure 4.** (a) Schematic of binding TOA to $Au_{22}(SG)_{18}$ clusters (Au, blue; S, green), (b) digital photograph of $Au_{22}(SG)_{18}$ in water and TOA-$Au_{22}$ clusters in toluene under long-wavelength UV lamp irradiation (365 nm), and (c) luminescence spectra of $Au_{22}(SG)_{18}$ in water and TOA-$Au_{22}$ in toluene. Also, shown in the graph is the fluorescence spectrum of Rhodamine B (RhB, QY = 31%)[41] with the same optical density.

between the carboxylate anions of the $Au_{22}(SG)_{18}$ cluster in an aqueous phase and TOA cations in toluene is strong, so the TOA-bound $Au_{22}$ clusters readily transfer to the toluene phase within a few minutes (see Experimental Section for experimental details). The TOA-paired $Au_{22}$ clusters (TOA-$Au_{22}$) were found to be very stable in toluene and also soluble in many other organic solvents such as dichloromethane, ethanol, methanol, acetonitrile, etc.

SI Figure S5 shows the negative-mode ESI mass spectrum of TOA-$Au_{22}$ clusters. There are peaks observed at $m/z$ 2800−3000 that represent TOA-$Au_{22}$ ions with the overall charge of $5^-$, which is determined by the total number of counterions ($H^+$, $Na^+$, $TOA^+$) paired with the carboxylate of the glutathione ligands. As can be seen in the figure, the TOA-$Au_{22}$ cluster ions retain their original composition of $Au_{22}(SG)_{18}$, and they are likely generated by the dissociation of TOA cations. This indicates that the number of TOA cations paired with $Au_{22}(SG)_{18}$ is >13, which is also consistent with NMR analysis of the TOA-$Au_{22}$ clusters (SI Figure S6). The observed peaks at $m/z$ ~2993 Da match well with the isotope pattern of $[Au_{22}(SG)_{18}{}^0\text{-}16H^+\text{+}11TOA^+]^{5-}$, as compared in SI Figure S5b.

SI Figure S7 shows that the absorption spectra of $Au_{22}(SG)_{18}$ and TOA-$Au_{22}$ are almost identical, indicating that the paired cluster retains its original optical properties. In stark contrast, the luminescence intensity was drastically enhanced after being paired with TOA, as can be seen in Figure 4; the intensity increased nearly 9-fold, and a QY of 62% was observed for TOA-$Au_{22}$ clusters in toluene. Also, the luminescence maximum shifted to higher energies (~630 nm), suggesting that the binding of the gold shell with TOA altered the luminescent triplet state. It is noteworthy that these behaviors are distinctly different from the AIE observed for Au(I)−thiolate complexes,[26] which makes the TOA-$Au_{22}$ cluster unique.

It could be argued that there could be some solvent (toluene) contribution to the enhanced luminescence observed for the TOA-$Au_{22}$ clusters in Figure 4. To evaluate the solvent effect, $Au_{22}(GS)_{18}$ clusters were phase-transferred into toluene using a different counterion, cetyltrimethylammonium (CTA), instead of TOA. The luminescence of the CTA-paired $Au_{22}$ clusters in toluene exhibited, however, essentially no enhancement compared to that of $Au_{22}(GS)_{18}$ clusters in water (Figure 5a). This result indicates that the luminescence enhancement

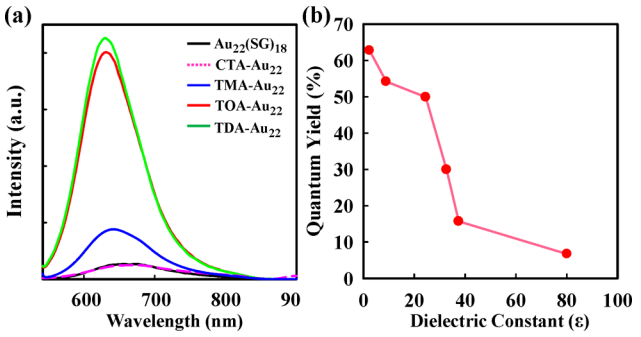


**Figure 5.** (a) Luminescence spectra of $Au_{22}(SG)_{18}$ paired with quaternary ammonium cations with different chain length: $Au_{22}(SG)_{18}$ in water (black) and CTA- (pink), TMA- (blue), TOA- (red), and TDA-paired (green) $Au_{22}$ clusters in toluene. All cluster solutions have the same absorbance (0.025) at 514 nm and are excited at 514 nm. (b) Luminescence of TOA-$Au_{22}$ clusters in various solvents with different dielectric constants: toluene ($\varepsilon$ = 2.38), dichloromethane ($\varepsilon$ = 8.93), ethanol ($\varepsilon$ = 24.5), methanol ($\varepsilon$ = 32.7), and acetonitrile ($\varepsilon$ = 37.5) and $Au_{22}(SG)_{18}$ in water ($\varepsilon$ = 80).

observed for the TOA-$Au_{22}$ clusters was not due to the organic solvent but rather to the presence of TOA paired to the $Au_{22}$ clusters. Since CTA has only one chain of long alkyl groups, there could be fewer interactions between them, which presents a small influence on rigidifying the structure compared to the bulky TOA. This result also rules out the possibility of luminescence enhancement by the electric field effect induced by the bound TOA cations, as the similar effect would be expected for the CTA-paired $Au_{22}$ clusters.

When the TOA-$Au_{22}$ was phase-transferred back to the aqueous phase by adding tetramethylammonium decanoate to the TOA-$Au_{22}$ clusters in toluene, the luminescence drastically decreased and exhibited a similar quantum yield of ~7%, indicating that there was no size change involved in the phase transfer reactions, unlike other metal clusters,[42] and that the luminescence enhancement effect was solely caused by TOA binding. Whereas the enhanced luminescence is mainly induced by TOA, luminescence of TOA-$Au_{22}$ exhibits interesting solvent dependence, as shown in Figure 5b. That is, the luminescence significantly decreased with increased dielectric constant of the solvent. This can be understood by weakening the effect of ion pairing in polar media. As the ion pairing becomes weakened in polar media, the rigidity of the gold shell drastically decreases and the luminescence relaxation then occurs at the solvent-stabilized $T_2$ state.

Further time-resolved luminescence measurements were carried out for TOA-$Au_{22}$ clusters to understand if the binding of TOA altered the radiative and nonradiative relaxation at room temperature. Nanosecond time-resolved luminescence measurements have shown a drastically increased lifetime of


DOI: 10.1021/jacs.5b04210
J. Am. Chem. Soc. 2015, 137, 8244−8250

2.44 $\mu$s for TOA-$Au_{22}$, a greater than 6-fold increase compared to that in the 380 ns for $Au_{22}(GS)_{18}$ clusters (SI Figure S8). It is interesting to note that the microsecond-scale lifetime of TOA-$Au_{22}$ is comparable with that of $Au_{22}(SG)_{18}$ at 77 K (4.75 $\mu$s). The enhanced luminescence with a maximum shift from 665 to 630 nm and increased lifetime are similar to those observed for $Au_{22}(GS)_{18}$ clusters with reduced temperature, indicating that rigidifying of the gold shell is possible when bound with TOA. In addition, the $^1$H NMR resonance peaks for $CH_2$ protons (2.0−2.7 ppm) of glutathione for TOA-$Au_{22}$ become severely broadened, as can be seen in SI Figure S6, indicating that the shell becomes rigidified upon binding with TOA.

The chain length effect of quaternary ammonium cations on the luminescence of paired $Au_{22}$ clusters clearly confirms that the luminescence enhancement is due to enhanced rigidity of the gold shell. As expected, the $Au_{22}(GS)_{18}$ ion paired with tetradecylammonium (TDA) cations showed an emission (QY = 66%) even brighter than that with TOA-$Au_{22}$, as shown in Figure 5a. However, the phase transfer reactions from water to toluene with shorter quaternary ammonium cations were unsuccessful. We have instead carried out a cation exchange reaction of the preformed TOA-$Au_{22}$ clusters with an excess amount of quaternary ammonium cations with a shorter alkyl chain such as tetramethylammonium (TMA). As can be seen in Figure 5a, the luminescence intensity significantly decreased when the TOA cations are replaced with TMA cations in toluene. These results evidently confirm that the enhanced luminescence intensity is strongly associated with the rigidity induced by pairing with bulky counterions. The above results unambiguously show that ultrabright luminescence observed for the TOA-$Au_{22}$ clusters originated from rigidifying the Au(I)−thiolate shell induced by pairing with bulky counterions such as TOA and TDA.

It is interesting to note that there is also TOA binding effect observed for a weakly luminescent $Au_{25}(SG)_{18}$ cluster (SI Figure S9). TOA-paired $Au_{25}(SG)_{18}$ clusters were prepared similarly to the TOA-$Au_{22}$ clusters.[40] Although the luminescence of a resulting cluster remains weak (QY ~ 0.6%), there was about a 6-fold enhancement observed for $Au_{25}(SG)_{18}$ upon pairing with TOA, as shown in SI Figure S9b. The lifetime also increased from 160 to 940 ns upon binding with TOA (SI Figure S10). These results suggest that the luminescence arises from the gold shell, and there is a rigidifying effect observed even for $Au_{25}(SG)_{18}^-$. When the well-separated dimeric gold shell structure of the $Au_{25}(SG)_{18}$ cluster is considered,[18] however, the aurophilic effect is unlikely in this cluster and thus the luminescence can be ascribed to the ligand-to-metal charge transfer (LMCT) effect, as proposed by Jin and co-workers,[13] rather than the LMMCT effect.[32,33]

What is the design strategy for highly luminescent metal clusters then? Comparison of similarly sized $Au_{22}(SG)_{18}$ and $Au_{25}(SG)_{18}$ clusters manifests that the aurophilic effect in the gold shell and ensuing LMMCT relaxation is important for higher luminescence. Further enhancement can be achieved by rigidifying the gold shell. In the present work, we have shown that it is possible to achieve luminescence QY greater than 60% by rigidifying the gold shell by lowering the medium temperature or binding with bulky groups. This approach for attaining higher luminescence could be used for other gold clusters with luminescent gold shells. The highly luminescent clusters offer promise for biomedical imaging and display applications. Furthermore, the enhancing strategy of the gold shell emission can be effectively used for the detection of proteins and other biologically relevant materials that can change the environment around the gold shell. This work opens new avenues to the use of highly luminescent gold clusters in such applications.

## EXPERIMENTAL SECTION

**Materials.** Gold(III)chloride trihydrate ($HAuCl_4 \cdot 3H_2O$, reagent grade), reduced L-glutathione (GSH, ≥98%), sodium borohydride ($NaBH_4$, 99%), tetraoctylammonium bromide (TOABr, 98%), cetyltrimethylammonium bromide (CTABr, ≥98%), tetramethylammonium bromide (TMABr, 98%), triza base (≥99%), glycine (for electrophoresis, ≥99%), acrylamide/bisacrylamide (bio reagent, 40%), and Rhodamine B were purchased from Sigma-Aldrich. Tetradecylammonium bromide (TDABr, ≥98%) was purchased from Tokyo Chemical Industry Co. Sodium hydroxide (NaOH, 98%), hydrochloric acid (HCl, 35−37%), isopropyl alcohol (IPA, 99%), and ACS-grade toluene, acetonitrile, ethanol, and methanol were purchased from Burdick and Jackson. Water was purified using a Millipore Milli-Q system (18.2 MΩ·cm). All of the chemicals were used as received without further purification.

**Methods.** UV−vis absorption and photoluminescence spectra of the $Au_{22}(SG)_{18}$ and TOA-paired $Au_{22}(SG)_{18}$ clusters (TOA-$Au_{22}$) were recorded by using a Shimadzu UV−vis−NIR spectrophotometer (UV-3600) and Scinco fluorescence spectrometer (Fluoro Mate FS-2), respectively. TEM images were collected on a JEOL electron microscope (JEM-2010). TEM samples were prepared by drop-casting a toluene solution of TOA-paired $Au_{22}(SG)_{18}$ clusters (1 mg/1 mL) on a 400 mesh Formvar/carbon-coated copper grid (01814-F, Ted Pella) and drying for 2 h at room temperature before imaging. The chemical composition of isolated $Au_{22}(SG)_{18}$ clusters was analyzed by using ESI mass spectrometry (LTQ Orbitrap XL, Thermo Scientific) in negative-ion mode (flow rate, 5.0 $\mu$L/min; capillary voltage, 4.2 kV; capillary temperature, 180 °C; $m/z$ range, 1000−4000). The samples were prepared in ultrapure water at a concentration of 5 mg/5 mL and directly injected into the mass spectrometer. The molecular formula of the TOA-paired $Au_{22}$ was analyzed by an ESI mass spectrometer (compact Q-TOF, Bruker) in negative-ion mode (flow rate, 5.0 $\mu$L/min; capillary voltage, 3.0 kV; capillary temperature, 180 °C; $m/z$ range, 1000−3000). The samples were prepared in a mixture of toluene and acetonitrile at a concentration of 5 mg/5 mL and directly injected into the mass spectrometer. The isolated Au clusters were run through PAGE by Mini-PROTEAN Tetra Cell (Biorad) to verify the purity of the clusters. The homemade stacking gel and resolving gel were 4 and 30 wt %, respectively, and PAGE was processed for 2 h at 150 V until the bands were distinctly separated.

**Synthesis of $Au_{22}(SG)_{18}$ Clusters.** In a typical synthesis, an aqueous solution of 20 mM $HAuCl_4$ (12.5 mL) and 50 mM glutathione (GSH, 7.5 mL) was added to 230 mL of ultrapure water in a 500 mL Erlenmeyer flask (see SI for materials and methods). The mixture was then vigorously stirred for 2 min until the yellowish solution turned cloudy. After being stirred, the pH was adjusted to 12.0 using 1 M NaOH, which made the color of the solution turn clear yellow. Thereafter, diluted 0.1 mL of $NaBH_4$ (3.5 mM) was slowly added dropwise. The reaction solution was then stirred for 30 min. During the first 15 min, the solution slowly turned orange. Finally, the pH was adjusted to 2.5 to quench the $BH_4^-$ activity and stirred slowly (150 rpm) for 6 h at room temperature. The product solution was then rotary evaporated to near dryness. To isolate $Au_{22}(SG)_{18}$ from the raw product, solvent fractionation was conducted using water−IPA mixtures. Typically, the product was dissolved in 10 mL of water, and 12 mL of IPA was added to induce precipitation of large-sized nanoclusters, which was found to be $Au_{22}(SG)_{18}$ in this case. The precipitate was separated by centrifugation, and more IPA (1 mL) was added to the supernatant to induce additional precipitation of $Au_{22}(SG)_{18}$. This process was repeated until the supernatant was clear. Highly pure $Au_{22}(SG)_{18}$ clusters were predominantly obtained in the first precipitate and identified by using ESI mass spectrometry and UV−vis absorption spectrometry. This water-soluble $Au_{22}(SG)_{18}$ was found to be very stable for more than 6 months in aqueous solution.


DOI: 10.1021/jacs.5b04210
J. Am. Chem. Soc. 2015, 137, 8244−8250

**Synthesis and Characterization of Highly Luminescent TOA-$Au_{22}$ Clusters.** In a typical procedure, 10 mg of $Au_{22}(SG)_{18}$ dissolved in 10 mL of ultrapure water and 10 mg of TOABr (TOA/$Au_{22}(SG)_{18}$ = 18) in 1 mL of toluene were added to a 20 mL scintillation vial. The aqueous solution was then adjusted to pH 9.0, ensuring that the carboxyl groups of glutathione were anionic forms. The electrostatic interaction between the carboxylate anions of the glutathione ligand and the hydrophobic TOA cations in the toluene phase appeared to be quite strong so that the TOA-paired $Au_{22}$ clusters were readily transferred (within 3 min) to the toluene phase by hand-shaking the two immiscible solutions. After the toluene phase was separated into a new vial, 15 mL of ultrapure water was added to the toluene solution to remove any water-soluble impurities by shaking the two immiscible solutions. This step was repeated until nothing was extracted into water. The toluene solution of the purified TOA-paired $Au_{22}$ clusters (TOA-$Au_{22}$) was stored in a refrigerator until further use.

**Temperature-Dependent and Time-Resolved PL Measurements.** Temperature-dependent PL measurements were carried out in an Edinburgh spectrofluorimeter (F900S). The fluorimeter is coupled with an Optistat DN cryostat (Oxford Instruments), and the ITC temperature controller and a pressure gauge were used to conduct the temperature-dependent experiments from 77 to 313 K. The vacuum in the cryostat was maintained with a leybold turbo molecular pump. Spectra were taken at different temperatures after a wait period of 10 min. The error in temperature setting is ±0.5 K. The $Au_{22}(SG)_{18}$ sample was dissolved in a 65:35 glycerol/water mixture, and TOA-$Au_{22}$ samples were dissolved in ethanol for temperature-dependent PL measurements. All the samples were purged with $N_2$ to get rid of dissolved oxygen to omit the problems in solvent freezing temperatures as well as the effect of oxygen on phosphorescence lifetimes. Optical absorption measurements before and after temperature-dependent PL measurements have shown no change, suggesting the samples did not change during the measurements.

Time-resolved PL lifetime measurements were measured using a time-correlated single-photon counting technique after excitation at 503 nm with a diode laser excitation, and the measurements were carried out in an Edinburgh F900S spectrofluorimeter. Cooled Hamamatsu R-921P PMT was used as the detector. Temperature-dependent time-resolved PL measurements were also carried out using the same apparatus described above by changing the excitation source to a diode laser. Time-resolved luminescence measurements of the gold clusters were also studied using the femtosecond luminescence up-conversion technique described elsewhere.[28] Briefly, the up-conversion system used in our experiments was obtained from CDP Instruments, Inc., Russia. In the present investigation, studies were carried out with the second harmonic (400 nm) of the fundamental Ti:sapphire laser at 800 nm as the excitation source. Polarization of the excitation beam for the magic-angle fluorescence and anisotropy measurements was controlled using a Berek compensator, and the sample was continuously rotated with a rotating cell of 1 mm thickness. Horizontally polarized luminescence emitted from the sample was up-converted in a nonlinear crystal of $\beta$-barium borate using a pump beam at 800 nm, which first passed through a variable delay line. Fitting the Raman signal from water gave a sigma value of ~120 fs for instrument response. Spectral resolution was achieved using a double monochromator and photomultiplier tube. The excitation average power varied but was around 10 ± 0.3 mW, and an average collection time of 3 s was used for most wavelengths. No degradation of the sample was observed as the traces overlapped after each repetition, and the optical absorption measurements did not show any change before or after the measurements.

## ■ ASSOCIATED CONTENT

### Supporting Information

Additional figures of the characterization and further experimental results. The Supporting Information is available free of charge on the ACS Publications website at DOI: 10.1021/jacs.5b04210.

## ■ AUTHOR INFORMATION


### Corresponding Authors

*dongil@yonsei.ac.kr

*rama.guda@wmich.edu

### Author Contributions

§K.P. and V.D.T. contributed equally to this study.


### Notes

The authors declare no competing financial interest.

## ■ ACKNOWLEDGMENTS

D.L. acknowledges support by the Korea CCS R&D Center (KCRC) grant (NRF-2014M1A8A1074219), the NRF grants (NRF-2014R1A2A1A11051032 and 2011-0022975), and the Yonsei University Future-leading Research Initiative of 2014. G.R. acknowledges the support of ACS-PRF #53999-ND5 and Western Michigan University startup.

## ■ REFERENCES


(1) Alivisatos, P. *Nat. Biotechnol.* **2004**, *22*, 47.

(2) Mueller, A. H.; Petruska, M. A.; Achermann, M.; Werder, D. J.; Akhadov, E. A.; Koleske, D. D.; Hoffbauer, M. A.; Klimov, V. I. *Nano Lett.* **2005**, *5*, 1039.

(3) Waser, R. *Nanoelectronics and Information Technology: Advanced Electronics Materials and Novel Devices*, 3rd ed.; Wiley-VCH: Weinheim, Germany, 2003; Chapter 39.

(4) Michalet, X.; Pinaud, F. F.; Bentolila, L. A.; Tsay, J. M.; Doose, S.; Li, J. J.; Sundaresan, G.; Wu, A. M.; Gambhir, S. S.; Weiss, S. *Science* **2005**, *307*, 538.

(5) Medintz, I. L.; Uyeda, H. T.; Goldman, E. R.; Mattoussi, H. *Nat. Mater.* **2005**, *4*, 435.

(6) Derfus, A. M.; Chan, W. C. W.; Bhatia, S. N. *Nano Lett.* **2004**, *4*, 11.

(7) Mancini, M. C.; Kairdolf, B. A.; Smith, A. M.; Nie, S. *J. Am. Chem. Soc.* **2008**, *130*, 10836.

(8) Hardman, R. A. *Environ. Health Perspect.* **2006**, *114*, 165.

(9) Luo, Z.; Zheng, K.; Xie, J. *Chem. Commun.* **2014**, *50*, 5143.

(10) Liu, J.; Yu, M.; Zhou, C.; Yang, S.; Ning, X.; Zheng, J. *J. Am. Chem. Soc.* **2013**, *135*, 4978.

(11) Bigioni, T. P.; Whetten, R. L.; Dag, O. *J. Phys. Chem. B* **2000**, *104*, 6983.

(12) Huang, T.; Murray, R. W. *J. Phys. Chem. B* **2001**, *105*, 12498.

(13) Wu, Z. J.; Jin, R. *Nano Lett.* **2010**, *10*, 2568.

(14) Lee, D.; Donkers, R. L.; Wang, G. L.; Harper, A. S.; Murray, R. W. *J. Am. Chem. Soc.* **2004**, *126*, 6193.

(15) Liu, J.; Yu, M.; Ning, X.; Zhou, C.; Yang, S.; Zheng, J. *Angew. Chem., Int. Ed.* **2013**, *52*, 12572.

(16) Luo, Z.; Zheng, K.; Xie, J. *Chem. Commun.* **2014**, *50*, 5143.

(17) Udayabhaskararao, T.; Sun, Y.; Goswami, N.; Pal, S. K.; Balasubramanian, K.; Pradeep, T. *Angew. Chem., Int. Ed.* **2012**, *51*, 2155.

(18) Zheng, J.; Zhang, C. W.; Dickson, R. M. *Phys. Rev. Lett.* **2004**, *93*, 077402.

(19) Zheng, J.; Petty, J. T.; Dickson, R. M. *J. Am. Chem. Soc.* **2003**, *125*, 7780.

(20) Jin, R. *Nanoscale* **2010**, *2*, 343.

(21) Walter, M.; Akola, J.; Lopez-Acevedo, O.; Jadzinsky, P. D.; Calero, G.; Ackerson, C. J.; Whetten, R. L.; Grönbeck, H.; Häkkinen, H. *Proc. Natl. Acad. Sci. U.S.A.* **2008**, *105*, 9157.

(22) Negishi, Y.; Nobusada, K.; Tsukuda, T. *J. Am. Chem. Soc.* **2005**, *127*, 5261.

(23) Varnavski, O.; Ramakrishna, G.; Kim, J.; Lee, D.; Goodson, T., III. *J. Am. Chem. Soc.* **2010**, *132*, 16.

(24) Ramakrishna, G.; Varnavski, O.; Kim, J.; Lee, D.; Goodson, T., III. *J. Am. Chem. Soc.* **2008**, *130*, 5032.

(25) Tang, Z.; Xu, B.; Wu, B.; Germann, M. W.; Wang, G. *J. Am. Chem. Soc.* **2010**, *132*, 3367.




DOI: 10.1021/jacs.5b04210
*J. Am. Chem. Soc.* 2015, 137, 8244−8250

(26) Luo, Z.; Yuan, X.; Yu, Y.; Zhang, Q.; Leong, D. T.; Lee, J. Y.; Xie, J. *J. Am. Chem. Soc.* **2012**, *134*, 16662.
(27) Yu, Y.; Luo, Z.; Chevrier, D. M.; Leong, D. T.; Zhang, P.; Jiang, D.; Xie, J. *J. Am. Chem. Soc.* **2014**, *136*, 1246.
(28) Devadas, M. S.; Kim, J.; Sinn, E.; Lee, D.; Goodson, T., III.; Ramakrishna, G. *J. Phys. Chem. C* **2010**, *114*, 22417.
(29) Devadas, M. S.; Bairu, S.; Qian, H.; Sinn, E.; Jin, R.; Ramakrishna, G. *J. Phys. Chem. Lett.* **2011**, *2*, 2752.
(30) Devadas, M. S.; Thanthirige, V. D.; Bairu, S.; Sinn, E.; Ramakrishna, G. *J. Phys. Chem. C* **2013**, *117*, 23155.
(31) Lane, L. B. *Ind. Eng. Chem.* **1925**, *17*, 924.
(32) Yam, V. W. W.; Lo, K. K. W. *Chem. Soc. Rev.* **1999**, *28*, 323.
(33) Cha, S.-H.; Kim, J.-U.; Kim, K.-H.; Lee, J.-C. *Chem. Mater.* **2007**, *19*, 6297.
(34) Arbeloa, T. M.; Arbeloa, F. M.; Tapia, M. J.; Arbeloa, I. M. *J. Phys. Chem.* **1993**, *97*, 4704.
(35) Bhaskar, A.; Ramakrishna, G.; Lu, Z.; Twieg, R.; Hales, J. M.; Hagan, D. J.; Stryland, E. V.; Goodson, T., III. *J. Am. Chem. Soc.* **2006**, *128*, 11840.
(36) Ramakrishna, G.; Bhaskar, A.; Goodson, T., III. *J. Phys. Chem. B* **2006**, *110*, 20872.
(37) Ramakrishna, G.; Goodson, T., III. *J. Phys. Chem. A* **2007**, *111*, 993.
(38) Turro, N. J. *Modern Molecular Photochemistry*; University Science Books: New York, 1991.
(39) Wei, Z.; Gu, Z.-Y.; Arvapally, R. L.; Chen, Y.-P.; McDougald, R. N., Jr.; Ivy, J. F.; Yakavenko, A. A.; Feng, D.; Omary, M. A.; Zhou, H.-C. *J. Am. Chem. Soc.* **2014**, *136*, 8269.
(40) Kwak, K.; Lee, D. *J. Phys. Chem. Lett.* **2012**, *3*, 2476.
(41) Magde, D.; Rojas, G. E.; Seybold, P. G. *Photochem. Photobiol.* **1999**, *70*, 737.
(42) Yuan, X.; Luo, Z.; Zhang, Q.; Zhang, X.; Zheng, Y.; Lee, J. Y.; Xie, J. *ACS Nano* **2011**, *5*, 8800.


DOI: 10.1021/jacs.5b04210
*J. Am. Chem. Soc.* 2015, 137, 8244−8250